Available online at www.sciencedirect.com
ScienceDirect
Scripta Materialia 58 (2008) 691–694
Scripta MATERIALIA
www.elsevier.com/locate/scriptamat

Dynamic recrystallization in the shear bands of Fe–Cr–Ni monocrystal: Electron backscatter diffraction characterization

Yongbo Xu,[a,*] H.J. Yang[a] and Marc André Meyers[b]

[a] *Shenyang National Laboratory for Materials Sciences, Institute of Metal Research, Chinese Academy of Sciences, Shenyang 110016, China*

[b] *University of California, San Diego, La Jolla, CA 92093-0411, USA*

Received 18 October 2007; revised 19 November 2007; accepted 5 December 2007
Available online 8 January 2008

An investigation was carried out into the microstructural evolution of the adiabatic shear bands generated under high-strain rate loading in a Fe–Cr–Ni single crystal. The results show that the distribution in plasticity on both sides of the bands during propagation is inhomogeneous, and recrystallization with an average grain diameter of 0.2 μm may occur. These distortion-free nanograins are believed to form as the result of dynamic recrystallization.

Keywords: Dynamic deformation; Adiabatic shear band; Recrystallization; Electron backscatter diffraction; Fe–Cr–Ni monocrystal

Adiabatic shear bands are regions of highly localized deformation, and the presence of recrystallized grains in the bands induced by high-strain rates has been reported in a number of different materials [1–9]. There are two methods to characterize recrystallization occurring in the shear bands: measurement of the temperature rise, and transmission electron microscopy (TEM) observation. Due to the difficulties encountered in measuring temperature rise during dynamic loading, the temperatures detected are scattered [8–12] and most of these measurements are not sufficient to prove the occurrence of recrystallization in the band. The small width of the bands (of the order of 1–200 mm) renders microstructural examination difficult. Electron backscatter diffraction (EBSD) in conjunction with a recently developed field emission scanning electron microscope exhibits many advantages in determination of the microstructural evolution of the bands. It can allow a direct quantitative analysis of subgrains and substructures as small as 0.2 μm, and gives more accurate measurements of subgrain/substructure size, misorientation and the distribution of boundary orientation than conventional imaging methods. These measurements can be made more easily than in a transmission electron microscope. However, only a few studies in microstructural evolution of the bands have been reported using EBSD [13–17]. Perez-Prado et al. [13] and Xue et al. [14] have investigated microstructural evolution of bands generated under high-strain rates by EBSD, but did not find recrystallized grains. Lins et al. [15] and Martinez et al. [16], however, have characterized recrystallization by EBSD in the bands of Ti–6Al–4V and interstitial-free steel, respectively. More recently, by using high-resolution EBSD techniques, dynamic recrystallized grains with an average grain of 200 nm in the bands in SS304 stainless steel have been found [17,18]. The goal of this paper is to investigate by EBSD the microstructural evolution of the shear bands generated in Fe–Cr–Ni alloy single crystal which was dynamically deformed (strain rate $\sim 10^4\ s^{-1}$) by the collapse of an explosively driven, thick-walled cylinder under prescribed initial temperature and strain conditions.

A single crystal of Fe–15Cr–15Ni, grown at the Advanced Research and Development Laboratory at Pratt & Whitney Aircraft (West Palm Beach, FL), was chosen for this study.

Figure 1 shows a shear band which initiates at the internal surface, and propagate along the shear direction. It can be seen that the shear band has a well-defined boundary on one side, and is divergent on the other side of the band. This kind of phenomenon is also observed in steels [3] and Ti [19], and can be explained by the experimental result of Stone and Thomas [20]. They have determined the stress–strain response of Fe–Cr–Ni monocrystal in three directions of $[100]_\gamma$, $[1\bar{1}0]_\gamma$,

* Corresponding author. E-mail: ybxu@imr.ac.cn

1359-6462/$ - see front matter © 2007 Acta Materialia Inc. Published by Elsevier Ltd. All rights reserved.
doi:10.1016/j.scriptamat.2007.12.006

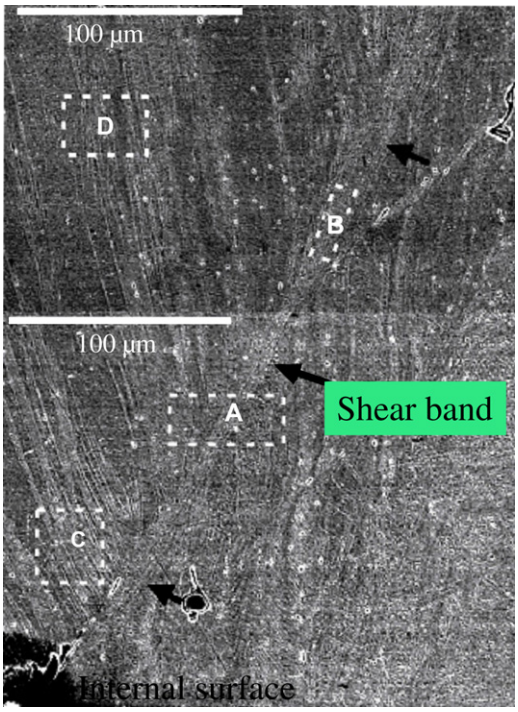

Figure 1. The shear bands generated under high-strain rate ($\sim 10^4\ s^{-1}$) in Fe–Cr–Ni alloy monocrystal.

$[\bar{1}\,\bar{1}\,2]_\gamma$ and $[\bar{2}\,\bar{1}\,3]_\gamma$, and found that the crystallographic anisotropy creates a mechanical anisotropy in the monocrystal. The [100] orientation, for example, has four slip systems with identical Schmid factors, and therefore a higher yield stress, and, thus, this direction shows a greater resistance to collapse [20].

The EBSD characterization was performed on several regions selected as shown in Figure 1 (white square marked A, B, C and D). Figure 2 is the EBSD map taken from an area (marked by square A in Fig. 1) crossing the bands. They are shown in Euler contrast (Fig. 2a) and in Kikuchi contrast (Fig. 2b). It is clear that an apparent shear band 3 μm wide is immediately seen, in which a great number of distortion-free and equiaxed grains appear. This kind of characteristic structure is proposed to be the result of the occurrence of recrystallization in the bands. EBSD characterization inside the band is shown in detail in Figure 3 where they are shown in a Euler angle map (a), a grain boundary map (b), in Kikuchi contrast (c) and in a {100} pole figure (d). It is immediately apparent that the equiaxied grains with high-angle grain boundaries (HAGBs) (Fig. 3b) are well developed and no obvious texture is shown in the {100} pole figure (Fig. 3d). The grain size distribution in the band is shown in Figure 3e, and the relative comparison of the misorientation angles of the regions inside and outside the band, and interfacial area near the band, is shown in Figure 3f. One can see clearly that most of the grains are about 100 nm in size, and the average size of the grains is about 200 nm (Fig. 3e). Boundary misorientations, which are readily obtainable from EBSD, enable the distribution of grain boundary type to be easily determined. Therefore, the relative comparison of the low-angle grain boundary (LAGB) fraction is shown in Figure 3f, from which it is found that the fraction of the LAGBs inside the band is only about 26%. In other words, most of the new recrystallized grains have HAGBs, and in two other regions, near and far away from the bands, the fractions of LAGBs are about 70% and 95%, respectively. This further proof that the region outside the band remains in the initial state, and the region near the band undergoes severe deformation. Figure 4 shows EBSD maps of the interfacial region (white square C in Fig. 1) near the band. These are the Euler angle map (a), the grain boundary map (b), and the {111},{110} and {100} pole figures (c). It can be seen that the orientation ⟨100⟩ (colored in red[1]) outside the band is in good agreement with the starting single-crystal orientation (⟨100⟩). The substructures (colored in orange) just below the band have an orientation ⟨111⟩ which is parallel to the normal direction (ND) in the {111} pole figure, and the substructures (colored in red) have an orientation ⟨100⟩ parallel to the ND. However, misorientations between them (colored in orange and blue) have LAGBs of about 1–3°. In Figure 4 HAGBs with misorientation angles larger than 15° are shown as black lines, and twin boundaries (TBs) with misorientation angles of $60 \pm 5°$, and LAGBs with misorientation angles of 1–15° are shown as red and green lines, respectively. It is clearly shown that as a consequence of high-strain rate deformation, the structures in this region near the band are deformed into substructures, and these substructures are bent, elongated and rotated relative to the shear direction. It is expected, therefore, that these elongated substructures observed very near the band are exactly the same as those found in the initial single crystal before recrystallization. It is also found that abundant TBs with misorientation angles of $60 \pm 5°$ immediately appear in this interfacial region, implying that twinning is an important deformation mechanism in the region near the shear bands. Figure 5 shows EBSD map of the region (marked by square D) far away from the band: these are shown as a Kikuchi band contrast map (Fig. 5a), a Euler angle map (Fig. 5b), and as the {100} pole figure (Fig. 5c). It can be seen that there are a great number of LAGBs with misorientation angles of 1–2° shown by white lines, and a few green lines represent misorientation angles of 2–15°. These imply that the majority of misorientations are low angles which are less than 2°. Figure 5c shows the {100} pole figure obtained from this region, indicating that the specimen normal is nearly parallel to the [100] direction, which is exactly the direction of the initial single crystal, indicating that this region basically retains the initial single-crystal structure with slight deformation. It is interesting to find that a completely similar evolution in microstructure to that of the present study also occurs in 304 stainless steel [21]. The present observation appears to suggest a rotational dynamic recrystallization mechanism [22]. Based on dislocation dynamics and the present observations, it is reasonable to propose a model describing a mechanism for dynamic recrystallization

[1] For interpretation of colors in Figs. 1–6, the reader is referred to the web version of this article.

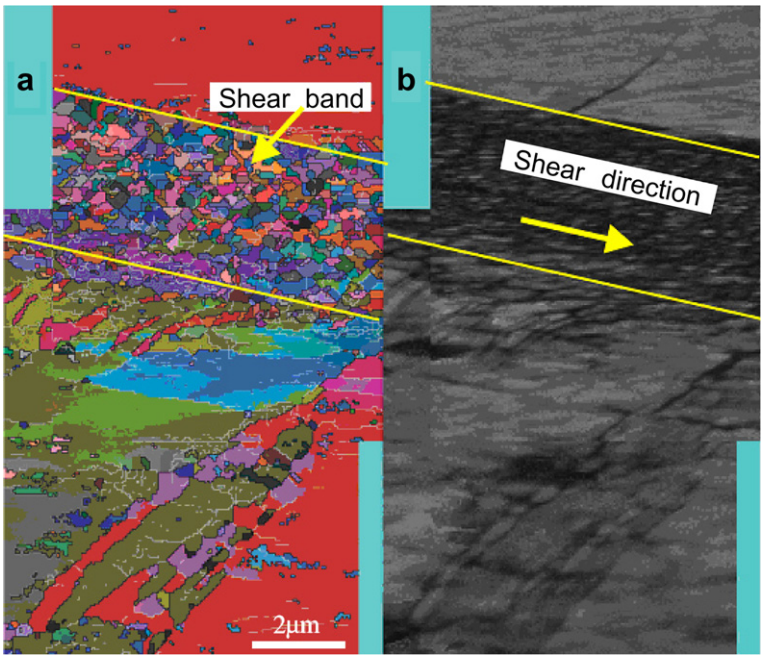

Figure 2. EBSD map of an area crossing the shear band, consisting of a shear band, an interfacial region near the band, and an area outside the band in Fe–Cr–Ni monocrystal. Step size: 0.05 μm; angular resolution: 1°.

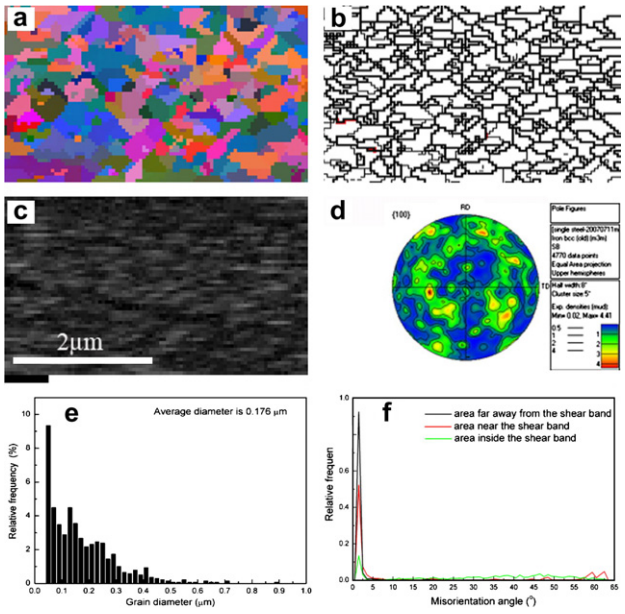

Figure 3. EBSD map inside the shear band: (a) Euler angle map, (b) grain boundary map, (c) Kikuchi contrast, (d) {100} pole figure, (e) grain size distribution inside the band, and (f) relative comparison of the misorientation angle distribution of the three regions: inside and outside of the band, and near the band.

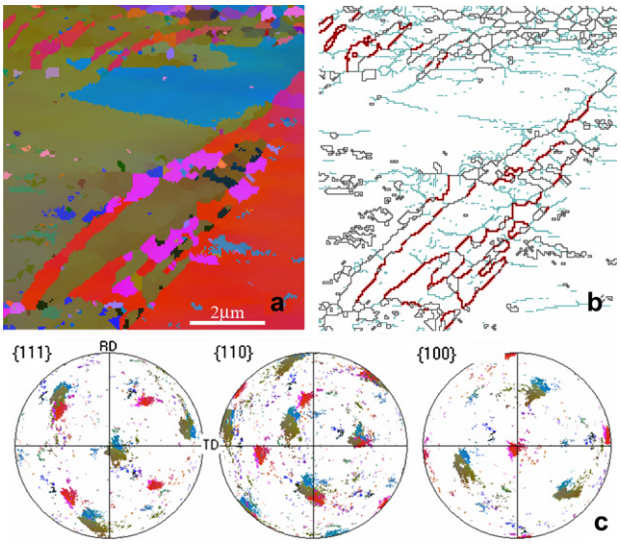

Figure 4. EBSD map of the area near the shear band: (a) Euler angle map, (b) grain boundary map, and (c) {111}, {110} and {100} pole figures.

occurring in the bands of the Fe–Cr–Ni monocrystal as shown in Figure 6. The dislocation distribution is homogeneous before deformation (a,b); as a consequence of dynamic deformation, the original grains are elongated into substructures (c,d); dislocations accumulate at substructure boundaries, and elongated substructures break up (e); the sub-boundaries reorient (f); there is an increase in orientation difference at boundaries and then rotation of sub-boundaries and formation of recrystallized grains with HAGBs (g,h). This model is, in fact, in good agreement with those proposed by Li et al. [21] and Meyers and co-workers [23].

In summary, this study has demonstrated that the distribution in plasticity on both sides of the bands is inhomogeneous and recrystallization may occur in the shear bands induced during high-strain rate loading in Fe–Cr–Ni monocrystal. These distortion-free nanograins in the bands appear to be the result of dynamic recrystallization occurring during localization, and can be explained by the mechanism of rotational recrystallization.

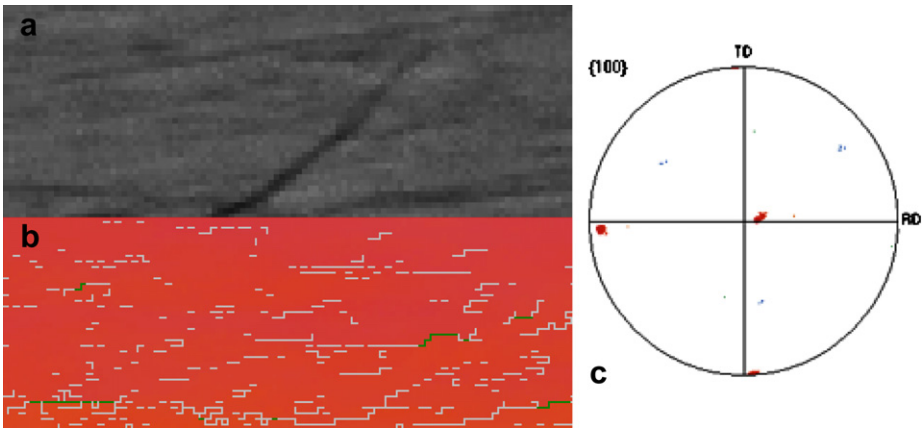

Figure 5. EBSD map outside the shear band: (a) Kikuchi band contrast map, (b) Euler angle map and (c) {100} pole figure. The white lines and green lines in (b) indicate misorientations of 1–2° and 2–15°, respectively.

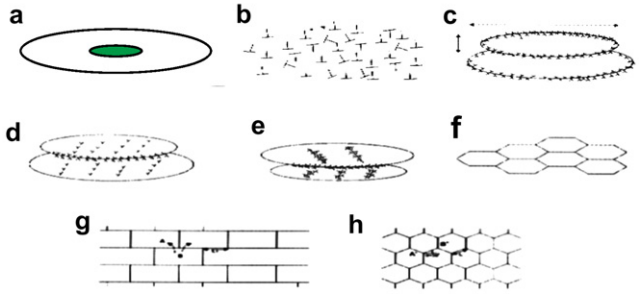

Figure 6. Schematic illustration of recrystallization in the band induced by high-strain rates in Fe–Cr–Ni monocrystal.

[1] C. Zener, J.H. Hollomom, J. Appl. Phys. 15 (1944) 22.
[2] H.C. Rogers, Annu. Rev. Mater. Sci. 9 (1979) 283.
[3] M.A. Meyers, Y.B. Xu, Q. Xue, M.T. Perez-Prado, T.R. McNelley, Acta Mater. 51 (2003) 1307.
[4] L.E. Murr, K.P. Staudhammer, S.S. Hecker, Metall. Trans. A 13A (1982) 627.
[5] C.M. Glass, G.M. Moss, S.K. Golaski, in: P. Shewmon, V.F. Zacakay (Eds.), Response of Metals to High Velocity Deformation, Wiley Interscience, New York, 1961, p. 115.
[6] M.C. Mataya, M.J. Carr, G. Krauss, Metall. Trans. 13A (1982) 263.
[7] S.P. Timothy, Acta Mater. 35 (1987) 301.
[8] J.A. Hines, K.S. Vecchio, S. Ahzi, Metal. Trans. A29 (1998) 191.
[9] S.C. Liao, J. Duffy, J. Mech. Phys. Solids 46 (1998) 2201.
[10] K.A. Hartley, J. Duffy, R.H. Hawley, J. Mech. Phys. Solids 35 (1987) 283.
[11] J.H. Giovanola, Mech. Mater. 7 (1988) 59.
[12] A. Marchand, J. Duffy, J. Mech. Phys. Solids 36 (1988) 59.
[13] M.T. Perez-Prado, J.A. Hines, K.S. Vecchio, Acta Mater. 49 (2001) 2905.
[14] Q. Xue, J.F. Bingert, B.L. Henrie, G.T. Gray III, Mater. Sci. Eng. A, in press.
[15] J.F.C. Lins, H.R.Z. Sandim, H.-J. Kestenbach, D. Raabe, K.S. Vecchio, Mater. Sci. Eng. A 457 (2007) 205.
[16] F. Martinez, L.E. Murr, A. Ramirez, M.I. Lopez, S.M. Gaytan, Mater. Sci. Eng. A 454-455 (2007) 581.
[17] Y.B. Xu, Y.L. Bai, Adv. Mech. 37 (2007) 497–561.
[18] H.J. Yang, Y.B. Xu, M.A. Meyers, Scripta Mater., submitted for publication.
[19] Q. Xue, M.A. Meyers, V.F. Nesterenko, Acta Mater. 50 (2002) 575.
[20] G. Stone, G. Thomas, Metall. Trans. 5 (1974) 2095.
[21] Q. Li, Y.B. Xu, Z.H. Lai, L.T. Shen, Y.L. Bai, Mater. Sci. Eng. A 276 (2000) 250.
[22] B. Derby, Acta Mater. 39 (1991) 955.
[23] Y.B. Xu, J.H. Zhang, Y.L. Bai, M.A. Meyers, Mater. Trans., in press.